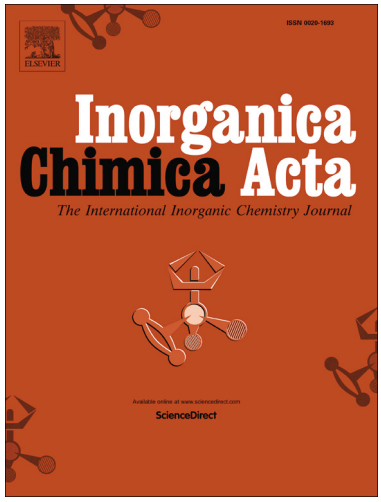

Research paper

Tetranuclear Cubane Cu_4O_4 complexes as prospective Anticancer Agents: Design, Synthesis, Structural Elucidation, Magnetism, Computational and Cytotoxicity Studies

Mohammad Usman, Farukh Arjmand, Rais Ahmad Khan, Ali Alsalme, Musheer Ahmad, Mousumi Sen Bishwas, Sartaj Tabassum

PII: S0020-1693(17)31439-1
DOI: https://doi.org/10.1016/j.ica.2017.12.039
Reference: ICA 18073

To appear in: *Inorganica Chimica Acta*

Received Date: 14 September 2017
Revised Date: 21 November 2017
Accepted Date: 29 December 2017

Please cite this article as: M. Usman, F. Arjmand, R.A. Khan, A. Alsalme, M. Ahmad, M.S. Bishwas, S. Tabassum, Tetranuclear Cubane Cu_4O_4 complexes as prospective Anticancer Agents: Design, Synthesis, Structural Elucidation, Magnetism, Computational and Cytotoxicity Studies, *Inorganica Chimica Acta* (2017), doi: https://doi.org/10.1016/j.ica.2017.12.039

Tetranuclear Cubane Cu_4O_4 complexes as prospective Anticancer Agents: Design, Synthesis, Structural Elucidation, Magnetism, Computational and Cytotoxicity Studies

Mohammad Usman,[1] Farukh Arjmand,[1] Rais Ahmad Khan,[2] Ali Alsalme,[2] Musheer Ahmad,[3] Mousumi Sen Bishwas,[4] and Sartaj Tabassum.[1]*

[1]*Department of Chemistry, Aligarh Muslim University, Aligarh-202002, India*
[2]*Department of Chemistry, College of Science, King Saud University, P.O. Box 2455, Riyadh 11451, KSA.*
[3]*Department of Applied Chemistry, ZHCET, Aligarh Muslim University, Aligarh, 202002, India.*
[4]*Physical and Material Chemistry Division, CSIR-National Chemical Laboratory, Dr. Homi Bhabha Road, Pune 411008, India.*

**Corresponding Author:*

Prof. Sartaj Tabssum, Tel: +91 9358255791, Email: tsartaj@yahoo.com

Abstract

Two new homometallic Cu_4O_4 cubane clusters **1** and **2** have been synthesized by self-assembly of copper(II) acetate and ligand, 2-[(2-Hydroxy-3-methoxy-benzylidene)-amino]-2-hydroxymethyl-propane-1,3-diol (**H_4L**) and characterized thoroughly by various spectroscopic techniques and single crystal X-ray diffraction analysis. Temperature-dependent magnetic susceptibility measurements have been performed to elucidate the antiferromagnetic and ferromagnetic nature in Cu_4O_4 clusters **1** and **2**, respectively. In vitro DNA binding studies of cubane clusters were carried out by employing optical spectroscopic techniques. Gel electrophoretic mobility assay performed to examine the nuclease activity of the complexes **1** and **2** with pBR322 DNA, and results revealed oxidative DNA cleavage via reactive oxygen species (ROS) species viz., $O_2^{\bullet-}$, $^1O_2$, etc. *In vitro* cell proliferation via MTT assay was studied to calculate the cytotoxicity of complexes **1** and **2**. The IC_{50} evaluated were ~ 20 μM in MCF-7 (Breast) and ~ 30-35 μM in HepG2 (Liver) cancer cell lines. Additionally, in the presence of **1**

and **2**, ROS and TBARS (Thiobarbituric acid reactive substance) levels amplified significantly, coupled with GSH (glutathione) levels in cancer lines. Hence, the results exhibited the major role of ROS in apoptosis induced by **1** and **2** clusters and validate their prospective to be efficient anticancer drug entities.

Keywords: Cu_4O_4 cubane complexes, Magnetism, DFT, DNA binding, Nuclease activity, Cytotoxicity.

1. Introduction

The synthetic design of multinuclear transition metal complexes is a thriving thrust area of research from the point of view of i) bioinorganic and ii) supramolecular chemistry [1]. Polynuclear complexes emerging from the aggregation of homo- or hetero-metal centers are the result of spontaneous self-assembly processes, capable of distinct recognition phenomenon towards the substrate. Interestingly, these complexes have shown remarkable biological, catalytic and magnetic properties [2].

Among the high nuclearity transition metal complexes, tetranuclear copper clusters having cubane-like Cu_4O_4 core are well studied and have received considerable attention [3, 4]. Tridentate Schiff base ligands are commonly used for the building of Cu_4O_4 cubane assembly. Three coordination sites of Cu(II) ion are filled by tridentate ligand, and a bridging ligand (azide, halides, hydroxide, pseudo-halides, oxalate, etc.) or μ-bridging alkoxo/phenoxo oxygen (self-assembly process) is used to obtain cubane structural frameworks [5].

Cu_4O_4 cubane clusters have been classified into structural types as a function of their topology and degree of distortion [6]. More recently, Alvarez et al. proposed a classification based on the dispersal of the six Cu···Cu distances with (2+4), (4+2) and (6+0) classes [3b]. The (2+4) and (4+2) cubane usually resembles systems in which Cu(II) ion has elongated octahedral or a square

pyramidal geometry, whereas (6+0) cubanes are assigned to the six equivalent faces unusual cores having geometry around Cu(II) ion trigonal bipyramidal in general. To date, only a limited number of alkoxo/phenoxo-bridge Cu(II) cubane structures have been reported [3c]. Apart from the structural novelty of cubane cores, the multinuclearity, and Cu_4O_4 cubane core are of great importance to the biologists in the area of drug design [7]. High metal nuclearity enhances the positive charge which in turn shows a greater propensity for negatively charged phosphate-sugar back bone of DNA and synchronized tuning between two or more metal centers enabling these complexes to bind nucleic acids multifold more selectively via non-covalent mode; further, it promotes DNA cleavage efficiency to achieve target specific chemotherapeutic agents [8]. In drug design strategy, high nuclearity component modulates pharmacological parameters and bears a disposition to alter the efficacy of the drug [7c].

Herein, we have designed and prepared Cu_4O_4 open cubane **1** cluster for the application in the area of drug design, particularly as an antitumor chemotherapeutic candidate. A very few literature reports have demonstrated the antitumor activity of Cu_4O_4 cubane tetranuclear clusters [9]. However, DNA binding and cleavage studies of some cubane complexes have been reported, yet there is much scope for more consolidated studies on design and synthetic strategy of novel cubane antitumor compounds [7a,9,10]. The presently synthesized Cu_4O_4 cubane clusters satisfactorily meet pharmacological drug discovery criteria i) high water solubility, ii) exhibit high DNA-binding propensity, snugly fit in the major groove of DNA helix as validated by docking iii) efficient DNA cleaving activity via ROS generation. The cytotoxic activity of cubane clusters **1** and **2** against HepG2 and MCF7 cancer cell lines were carried out by MTT assay, revealed good selectivity towards MCF7 breast cancer cell. As **1** showed selectivity

towards MCF7 breast cancer cell line, so we have explored the mechanistic pathways by carrying out assays to evaluate ROS generation, GSH depletion, and lipid peroxidation.

2. Experimental section

2.1. Materials and methods

2-hydroxy-3-methoxybenzaldehyde, 2-Amino-2-(hydroxymethyl)-1,3-propanediol, ethidium bromide (EB) and trimethylamine (Sigma-Aldrich), copper acetate monohydrate (Merck), supercoiled pBR322 DNA and 6X loading dye (Genie), were utilized as received and solvent were used as obtained. The disodium salt of calf thymus DNA was obtained from Sigma-Aldrich.

The chemicals, reagents, and diagnostics used for cytotoxic assays were purchased from Sigma-Aldrich. From Invitrogen, Life Technologies (USA), DMEM, solution of antibiotics/antimycotics and FBS were obtained.

On ThermoFinnigan CHN analysis was done. Eutech con 510 electronic (conductivity bridge) utilized to get the molar conductance at room temperature. PerkinElmer FT-IR spectrometers, was used to record FT-IR spectra. The EPR spectra were obtained by JEOL FA-200 continuous-wave spectrometer using Manganese (Mn) as standard (g = 2.0036). The absorption spectra were noted on PerkinElmer Lambda 35 UV/VIS spectrometer. Emission spectra were recorded on a Shimadzu RF5301PC spectrofluorophotometer using slit widths of 10/10 nm.

Magnetic readings were taken of polycrystalline powder sample by the help of a SQUID VSA dc magnetometer of Magnetic Property Measurement System (MPMS) from Quantum Design Inc., San Diego, CA, USA, armed with a superconducting magnet (7T). To affect our data accuracy, the magnetic value from the holder was insignificant. The dc magnetization M vs. T spectra were taken at 100 Oe with heating/cooling @ 2K/min. Magnetization vs. field loops was taken in a

field sweep from -50 to + 50 k Oe, @ 50 Oe/s. Axygen electrophoresis held with Genei power supply with a potential range of 50-100 V used for electrophoretic experiments, visualized and photographed by a Vilber-INFINITY gel documentation system.

2.2. Synthesis of ligand (H_4L)

A methanolic solution of 2-Amino-2-(hydroxymethyl)-1,3-propanediol (0.121g, 1 mmol) was added dropwise to the methanolic solution of 2−hydroxy−3−methoxybenzaldehyde (0.152 g, 1 mmol). The resulting mixture was refluxed at 80˚C for about 2 h until a pale yellow solid compound precipitated, filtered, washed with hexane and dried *in vacuo*.

Yield: 78%, M.P. 105 °C. Analysis Calculated for [$C_{12}H_{17}NO_5$] (%): C, 56.46; H, 6.71; N, 5.49; Found: C, 56.42; H, 6.78; N, 5.51. FT-IR (KBr pellet): 1643 υ(C=N); 1023 υ(O-CH_3); 2920 υ(C-H), 1023 ν(-OCH_3). UV−vis (1 x 10^{-4} M, MeOH, λ_{max} nm): 240, 292 and 416.

2.3. Synthesis of [$Cu_4(H_2L)_4 \cdot 2H_2O] \cdot 5H_2O$ (1)

A methanolic solution of 2-Amino-2-(hydroxymethyl)-1,3-propanediol(0.121g, 1 mmol) was added dropwise to the methanolic solution of 2−hydroxy−3−methoxybenzaldehyde (0.152 g, 1 mmol). The mixture solution was stirred for another 2 h at 80 °C and gives a clear dark yellow solution. $Cu(CH_3COO)_2 \cdot H_2O$ (0.199 g, 5 mmol) was added to the above reaction mixture in the presence of triethylamine (TEA) at pH 8-9 in MeOH/H_2O (90:10), which was further refluxed for 6h until a deep green solution resulted. After the reaction completion, the volume was reduced by heating on a hot plate and filtered hot. Then, the filtrate was left for slow evaporation, resulted in deep green colored crystals over a period of 6-7 days. These crystals were filtered, washed and air dried (Scheme 1).

Yield: 73%, M.P. 130 °C. Analysis calculated for $[Cu_4(H_2L)_4 \cdot 2H_2O] \cdot 5H_2O$ (%): C, 40.21; H, 8.02; N, 3.91; Found: C, 40.37; H, 8.11; N, 4.02. FT-IR (KBr pellet): 1624 cm^{-1} υ(C=N); 3373 cm^{-1} υ(O-H); 2936 cm^{-1} υ(Ar-H). UV-vis (1×10^{-4} M, MeOH, λ_{max} nm): 234, 280, 375, 645 nm. Molar conductance: Λ_M (1×10^{-3} M, DMSO): 6.03 Ω^{-1} cm^2 mol^{-1} (non-electrolyte).

2.4. Synthesis of $[Cu_4(H_2L)_4 \cdot 4H_2O]$ (2)

A methanolic solution of 2-Amino-2-(hydroxymethyl)-1,3-propanediol(0.121g, 1 mmol) was added dropwise to the methanolic solution of 2−hydroxy−3−methoxybenzaldehyde (0.152 g, 1 mmol). The solution mixture was allowed to stirr for 2 h at 80 °C to obtain a deep yellow clear solution. To this yellow solution, $Cu(CH_3COO)_2 \cdot H_2O$ (0.199 g, 1 mmol) solution in DMF and piperazine (0.086 g, 1 mmol) was added and refluxed ~4 h, until resulted into a dark green solution. When reaction got completed, the solution reduced in volume on a hot plate and filtered hot. Then, the filtrate is left for slow evaporation and after a period of 2-3 weeks, the deep green colored crystal was obtained. The crystals obtained were washed and air dried (Scheme 1).

Yield: 58%, M.P. 137 °C. Analysis calculated for $[Cu_4(H_2L)_4 \cdot 4H_2O]$ (%): C, 42.16; H, 7.08; N, 4.10; Found: C, 42.07; H, 7.12; N, 4.17. FT-IR (KBr): 1627 cm^{-1} υ(C=N); 3454 cm^{-1} υ(O-H); 2907 cm^{-1} υ(Ar-H). UV-vis (1×10^{-4}, MeOH, λ_{max} nm): 234, 280, 375, 625 nm. Molar conductance: Λ_M (1×10^{-3} M, DMSO): 6.16 Ω^{-1} cm^2 mol^{-1} (non-electrolyte).

2.5. Computational methodology

ORCA computational package was used for all the studies performed.[11] The single X-ray data was utilized to get geometry. By hybrid B3LYP functional by means of basis sets viz, Aldrich's def2-TZVP (for copper atom) and def2-SVP (for C, H, O, N atoms), single point energy calculations were done [12]. The computation was accelerated, by using RI (the

resolution of identity approximation) with the decontracted auxiliary coulomb fitting basis sets (def2-TZV/J or def2-SVP/J) and RIJCOSX (the chain-of-spheres approximation) to exact exchange as employed in ORCA [13].

The Autodock Vina (version 1.1.2.) [14] was used to perform molecular docking studies with B–DNA dodecamer (PDB ID: 1BNA) d(CGCGAATTCGCG)$_2$ was saved from the protein data bank (http://www.rcsb.org./pdb). For the minimum energy docked pose visualization, the Discovery Studio 4.1 and PyMol were used [15].

2.6. X-ray data collection and structure refinement

Single crystal X-ray data of synthesized Cu_4O_4 cubane clusters **1** and **2** were collected using MoK_α radiation (λ = 0.71073 Å) in diffractometer (Bruker SMART APEX CCD). The International Tables for Crystallography was inferred for the corrections in scattering factors (atoms), linear absorption coefficients, and anomalous dispersion [16]. The SAINT software was used to study the data integration and reduction [17]. The collected reflections were applied to empirical absorption correction with SADAB [18], and space group was determined using XPREP [19]. The direct methods using SHELXL-97 and SHELXL-2016/6 were used to solve the Cu_4O_4 cubane clusters **1** and **2** respectively, which were refined of F^2 by full-matrix least-squares using the SIR-97 programme package [20]. Only a few H atoms could be located in the difference Fourier maps in the structure. The rest were placed in calculated positions using idealized geometries (riding model) and assigned fixed isotropic displacement parameters. All non-H atoms were refined anisotropically. Several DFIX commands were used for fixing some bond distances in both complexes. The crystal and refined data are collected in Table 1 while selective bond distances and angles are given in Supporting Information, Table S1-S4.

Table 1. Crystal and structure refinement data for Cu_4O_4 cubane clusters **1** and **2**.

Parameters	**1**	**2**
Formula	$C_{48}H_{60}Cu_4N_4O_{27}$	$C_{48}H_{64}Cu_4N_4O_{24}$
Fw (g mol^{-1})	1379.16	1335.2
crystal system	Monoclinic	Tetragonal
space group	*P*21/*n*	*I*41/*a*
a (Å)	20.828(10)	18.609(2)
b (Å)	13.202(6)	18.609(2)
c (Å)	21.331(10)	15.425(2)
α (deg)	90	90
β(deg)	97.643(8)	90
γ (deg)	90	90
U ($Å^3$)	5813(5)	5341.6(13)
Z	4	16
ρ_{calc} (g/cm^3)	1.576	1.660
μ (mm^{-1})	1.532	1.660
F(000)	2832	2752
Temp (K)	296(2)	296(2)
measured reflns	27375	25013
unique reflns	4181	2016
GOF[a]	1.000	1.204
Final R[b] indices	$R1 = 0.0718$	$R1 = 0.1088$
[$I>2\sigma(I)$]	w$R2 = 0.2090$	w$R2 = 0.2245$
R[b] indices	$R1 = 0.1740$	$R1 = 0.1240$
(all data)	w$R2 = 0.2435$	w$R2 = 0.2325$
CCDC	1003913	1556830

[a]GOF is defined as $\{\Sigma[w(F_0^2-F_c^2)]/(n-P)\}^{1/2}$; n no. of data & "p" no. of parameters. [b]$R = \{\Sigma||F_0|-|F_c||/\Sigma|F_0|$, $wR^2 = \{\Sigma\, w(F_0^2-F_c^2)^2 / \Sigma\, w(F_0^2)^2\}^{1/2}$.

2.7. DNA interaction and cleavage experiments

The DNA binding studies were performed in Tris-HCl/NaCl (5:50) buffer at pH 7.4, using the standard protocols and with slight modification adopted by our laboratory in the past [21-24].

2.8. Biological experiments

All the biological experiments were carried out by our group with slight modifications in the standard protocols [22,25,26]

2.8.1. Cell lines and culture

In Brief, Both the cells HepG2 and MCF-7 cancer cells were cultured in DMEM in addition with FBS (10%), 0.2% $NaHCO_3$, and 1 mL/100 mL of 100X medium (antibiotic/antimycotic solution). At 37 °C with high humidity under 5% CO_2-95% air, the cells were maintained.

2.8.2 Cytotoxicity by the MTT assay

The protocol followed for MTT assay was previously reported by us [22]. Briefly, In 96 well culture plate, 1x 10^4 cells adhered to 24h in CO_2 incubator. Then, the from the stock of 5mg/mL in PBS of MTT added 10 µL to each cell suspension and incubated for 4h. After this supernatant discarded and DMSO (200 µL) to each well and gently mixed and read at 550 nm. Identical conditions were used for control, and IC_{50} values were calculated.

2.8.3. Cell Morphology

Inverted phase contrast microscope was used to take images of morphological changes observed by the compounds on MCF7 and HepG2 cells after treatment for 24 h.

2.8.4. Reactive oxygen species (ROS) generation

The protocol used to examine ROS generation is described earlier [22], using DCFH-DA dye as the fluorescent probe. After treatment cells for 24h washed with PBS and then were incubated with DCFH-DA (20 µM) for 1h in the dark. Lastly, by the help of fluorescence microscope, the cells were analyzed.

2.8.5. Intracellular Glutathione Depletion

The protocol used to evaluate Intracellular glutathione depletion was described earlier [22,25], Concisely, after cellular treatment protein is extracted from sonication with 1 mL TCA (10%) and cooled on ice for 1h and then centrifuged at 3000 rpm for 10 min. In 2 mL solution of Tris buffer (0.4 M) with 00.2 M EDTA supernatant is added and then 0.01M DTNB used to make up

to 3 mL. Later, at 37 °C for 10 min kept on shaking water bath, and the absorbance was read at 412 nm.

2.8.6. Lipid peroxidation assay

For this study, TBARS protocol was adopted [26]. Precisely, after treatment cells were centrifuged and then sonicated in 1.15% potassium chloride (ice cold) solution and centrifuged at 300 rpm for 10 min. Then 1 ml of supernatant is added to a mixture of TCA (15%), TBA (0.7%) and HCl (0.25N) called as TBA reagent (2 mL) and at 100 °C for 15 min was heated, in boiling bath. Further cooled and again centrifuges for 10 min at 1000rpm and the absorbance was measured at 550 nm.

3. Result and discussion

3.1. Synthesis and characterization

The multi-dentate Schiff base ligand **H_4L** was synthesiszed by simple condensation of 2-hydroxy-3-methoxybenzaldehyde with 2-Amino-2-(hydroxymethyl)-1,3-propanediol in MeOH. At room temperature in 1:1 molar ratio, H_4L with $Cu(CH_3COO)_2 \cdot H_2O$ were mixed and added triethylamine in methanol-water (90:10) at pH 8-9 yielded dark green colored cubane clusters 1 (Scheme 1). The reaction of **H_4L** with $Cu(CH_3COO)_2 \cdot H_2O$ along with piperazine in a 1:1:1 molar ratio and triethylamine at pH 8-9 in MeOH-DMF (80:20) at ambient temperature afforded a light green color compound that was crystallized into a new cubane cluster **2** (Scheme 1). Our efforts to control self-assembly process of POM-based clusters, using organo-cation is vital and perhaps could provide the basis to design, employing a crystal engineering approach. To achieve this target, we used organic amine cation viz. piperazine in the synthesis of complex **2**. The use of piperazine helps to isolate self-assembled POM species in one-pot reaction systems thus preventing their rapid aggregation into clusters having more stable uniform symmetrical

topology. The molecular structures of **1** and **2** were elucidated by using a single crystal X-ray diffraction study. The analytical techniques which were employed in the characterization of complexes include elemental analysis, solution electrical conductivity, FT-IR, UV-vis, X-band EPR and ESI-MS techniques.

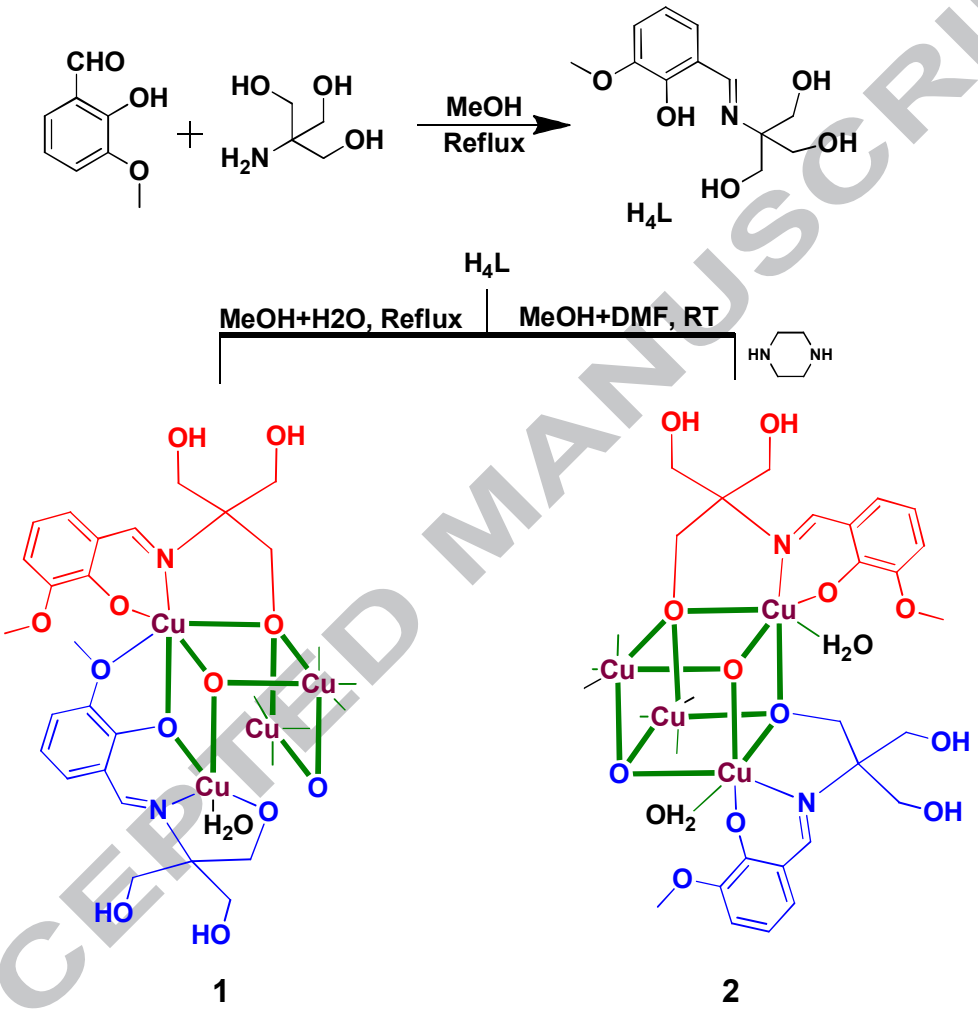

Scheme 1: Synthetic route of Cu_4O_4 open cubane **1** and Cu_4O_4 closed cubane **2** clusters. Coordinating ligand (H_2L^{2-}) of two copper center is omitted for clarity.

3.2. Crystal structure of $[Cu_4(H_2L)_4{\cdot}2H_2O]{\cdot}5H_2O$ (1)

The Single X-ray crystal structural technique revealed that complex **1** crystallized in the *P21/n* monoclinic space group possessing lattice parameters, a = 20.828 (10) Å, b = 13.202 (6) Å, c = 21.331 (10) Å, $\alpha = \gamma = 90^{o}$, β = 97.643 (8) Å. The asymmetric unit consists of four Cu(II) ion,

four H_2L^{2-} ligand, two coordinated and five lattice water molecules (Fig. 1). The complex **1** possesses open cubane-like core in which the four copper atoms are bridged by four oxygen atoms, two phenolate oxygen (O7 and O12) and two alkoxo oxygen atoms (O5, O20) from H_2L^{2-} ligands. Selected bond angles and lengths are given in Supporting Information, Table. S1 and S2. The Cu_4O_4 cluster comprises of four symmetry non-equivalent Cu(II) species, Cu1 and Cu4 cores reveal CuN_1O_5 coordination arrangement distorted octahedral shape, as evident by the angles around them, which deviate from 180^o and 90^o. The Cu1 atom is basically has alike to Cu4, and bonded with equatorial O2, N1, O5, and O7 atoms [Cu1-O6 2.373 Å; Cu1-O20 2.576 Å] of the $\mathbf{H_2L^{2-}}$ ligand moieties. The Cu4 atom has same coordination arrangement as ascribed for Cu1 atom and equitorial sites are satisfied by O20, N4, O17, O12 atoms [Cu4-O20 1.930 Å; Cu4-N4 1.976 Å; Cu4-O17 1.887 Å; Cu4-O12 2.001 Å], axial sites completed with O5 and O11 [Cu4-O5 2.588 Å; Cu4-O11 2.354 Å].

The penta-coordinated Cu2 signify CuN_1O_4 distorted square pyramidal geometry with $\tau = 0.02$, coordinated from O10, N2, O7, and O20 atoms [Cu2-O10 2.008 Å; Cu2-N2 1.958 Å; Cu2-O7 1.958; Cu2-O20 1.930Å] in equatorial positions of ligand $\mathbf{H_2L^{2-}}$ ligand moieties, while axial site engaged by O2W [Cu2-O2W 2.334 Å] of water molecule. Also, Cu3 metal core displayed CuN_1O_4 distorted square pyramidal coordination with $\tau = 0.12$, the equitorial position bonded to O15, N3, O12, and O5 [Cu3-O15 2.030 Å; Cu3-N3 1.984 Å; Cu3-O12 1.951 Å; Cu3-O5 1.939 Å] and O1W [Cu3-O1W 2.233 Å] of water molecule in an axial position.

In the Cu_4O_4 core, metal cores are interconnected through two oxygen phenoxo (μ_1-O7/O12) and two oxygen alkoxo (μ_2-O5/O20) atoms of four H_2L^{2-} ligand to produce a distorted single-open cubane core $[Cu_4(\mu_1\text{-}O)_2(\mu_2\text{-}O)_2]$ with idealized S4-symmetry with Cu···Cu separation in the

3.218 – 3.301 Å range (avg. 3.247), which are quite comparable to the values of similar Cu_4O_4 cubane clusters reported in the literature [18-20].

3.3. Crystal structure of [$Cu_4(H_2L)_4 \cdot 4H_2O$] (2)

Ssingle X-ray crystal exhibited that the complex **2** crystallized in the tetragonal I 41/a space group possessing lattice parameters, $a = b = 18.609$ (2) Å, $c = 15.425$ (2) Å, $\alpha = \beta = \gamma = 90^o$ per unit cell. The asymmetric unit consists of four Cu(II) ion, four ligand $\mathbf{H_2L^{2-}}$ moieties and four coordinated water molecules (Fig. 1b). The complex **2** portrayed as a closed cubane-like core in which four Copper atoms are linked by four alkoxo bridges oxygen atoms of ligands $\mathbf{H_2L^{2-}}$. Selected bond angles and lengths are given in Table. S3 and S4.

The Cu_4O_4 closed cubane clusters consist of four symmetry-equivalent Cu atoms, in a CuN_1O_5 coordination environment arranged in octahedral geometries. The coordination environment around Cu is filled by three alkoxo bridge oxygen atoms [Cu1-O3 1.933(7) Å], one phenolate O2 and an imine N1 atoms [Cu1-N1 1.946(10) Å; Cu1-O2 1.933(7) Å] of the $\mathbf{H_2L^{2-}}$ ligand and sixth coordination position was completed by a water molecule [Cu1-O1W 2.719 Å].

The four copper centers in the cluster are mutually interconnected via four alkoxo oxygen (μ_1-O3) atoms of four ligand $\mathbf{H_2L^{2-}}$ moieties to generate a single-closed cubane core [$Cu_4(\mu_1\text{-}O)_4$] with Cu···Cu separations in the range of 3.171- 3,473 Å, well corroborated with earlier reported

results [3].

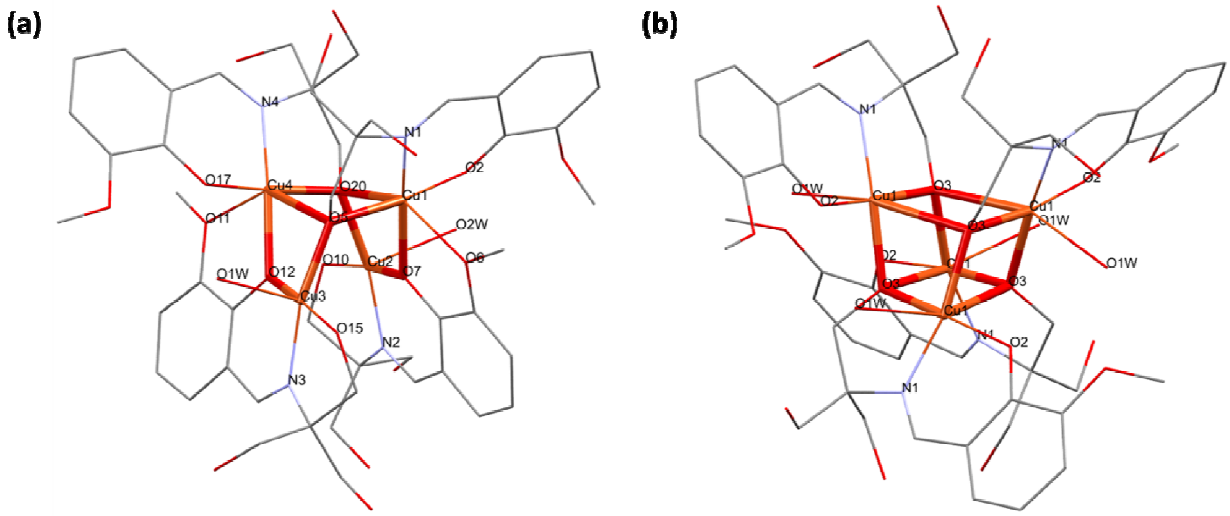

Fig. 1 X-ray molecular structures (a) Cu_4O_4 open cubane cluster, **1** (b) Cu_4O_4 closed cubane cluster, **2**. For clarity hydrogen atoms and lattice molecules have been omitted.

3.4. Spectroscopy

The IR spectrum of the free **H_4L** ligand exhibited IR absorptions at 1644, 1023, and 3342-3205cm^{-1} due to ν(C=N), ν(-OCH_3) and ν(O-H) vibrational modes, respectively, Supporting Information, Fig. S1 and S2 [20]. The ν(C=N) vibrational mode of complexes **1** and **2** w observed at 1624 and 1627cm^{-1} respectively, which are slightly lowered (15-20 cm^{-1}) relative to the free **H_2L^{2-}** ligand, revealing the coordination of imine nitrogen, Supporting Information, Fig. S3 and S4 [21]. Another substantial downward shift was observed in the stretching vibration of the C–OCH_3 group, from 959 to 923 cm^{-1} in **1** thereby indicating its coordination with the Cu atom. While an upward shift detected from 959 to 983 cm^{-1} in **2**, revealing the cubane core free from –OCH_3 coordination. Additionally, in the far-IR spectra of **1**, Supporting Information (Fig. S5), several absorption bands attributed to ν(Cu-O) frequencies *viz.*685, 399, 282 and 207 cm^{-1} originating from vibrations in the [Cu_4O_4] core were observed [21a].

The electronic spectra of **1** and **2** recorded in a MeOH solution, Supporting Information (Fig. S6), show very close resemblance and revealed three well-resolved absorption maxima at 234, 280 and 375 nm. The two sharp absorption bands centered at 234 and 280 nm correspond to π-π^* intraligand transitions while a broadband at 375 nm was assigned to the charge-transfer (LMCT) transitions of the phenolate or alkoxo oxygens to the copper ions. The bands centered at 645 nm and 625 in **1** and **2**, respectively, were assigned to the d-d transitions, Fig. S7 [21c].

The X-band EPR spectra for the polycrystalline powder of the Cu_4O_4 open cubane and closed cubane clusters **1** and **2** at room temperature (r.t) and liquid nitrogen (LN) temperature was recorded, Supporting Information, Fig. S8. No significant shift was observed in the g-values. In spectra of **1** an axial symmetrical signal with $g_{\parallel}$ at 2.33, $g_{\perp}$ at 2.03 and g_{av} at 2.13 {computed from the formula $g_{av}^2 = 1/3(g_{\parallel}^2+2g_{\perp}^2)$} was observed. The calculated values $g_{\parallel}$ and $g_{\perp}$ for **1** show the order as $g_{\parallel} > g_{\perp} > 2.0023$ which is indicative of the presence of an unpaired electron in the dx^2-y^2 orbital. The closed cubane cluster **2** exhibited a broad isotropic signal with g at 2.50 at 77K however, no signal was observed at room temperature. All these observations are in good agreement with the solid-state structure as determined by X-ray crystallography.

To obtain evidence for the stability of the Cu_4O_4 cluster **1** and **2** in solution, ESI-MS and UV-vis spectra were analysed. For **1,** ESI-MS exhibited *m/z* values of 1308.27 $[M\text{-}4H_2O]^+$ and 1336.16 $[M+H^+]$ for **2** (Fig. S9 and S10), corresponding to the stability of both the complexes in solution. The Fig. S11 of UV-vis spectra of **1** and **2** in Tris-HCl buffer at pH 7.4 and T 296 K, was recorded at various time intervals. The results displayed no significant changes nor in the intensity or position of absorption bands, and also demonstrating the stability of the Cu_4O_4 clusters **1** and **2** in solution phase.

3.5. Magnetic Properties

In **1**, χ_m increases monotonically from 300 K to 100 K and then a broad hump around 50 K was observed. Below this temperature, a very weak bifurcation in the ZFC-FC curve was observed, which is suggestive of antiferromagnetic interaction in the system. The $\chi_m T$ value at room temperature (300 K) was found to be 2.8 cm^3/mol.K which decreased monotonically as the temperature decreases and reached a value of 0.1 cm^3/mol.K at 3 K. The $1/\chi_m$ versus T plot indicates a very strong antiferromagnetic coupling with Weiss constant of -240 K as depicted in Fig. 2 and 3.

Similarly, in **2**, χ_m increased rapidly below 50 K till it reaches 3K. A very feeble bifurcation around 60 K was observed in the ZFC-FC magnetization data (Fig. 2, inset) which implicated the presence of extremely weak ferromagnetic interaction between the Cu(II) ions in the cubane complex. The observed $\chi_m T$ value at room temperature (300 K) was found to be 3.2 cm^3/mol.K which almost remained constant till the temperature decreased to 100 K and then after a short increase the $\chi_m T$ value decreased sharply to reach the value of 2.6 cm^3/mol.K at 3 K. The $1/\chi_m$ versus T plot in the **2** indicated that this complex obeyed the Curie-Weiss law in the whole measured temperature range and the Weiss constant was found to be ~-1 K showing an extremely weak interaction.

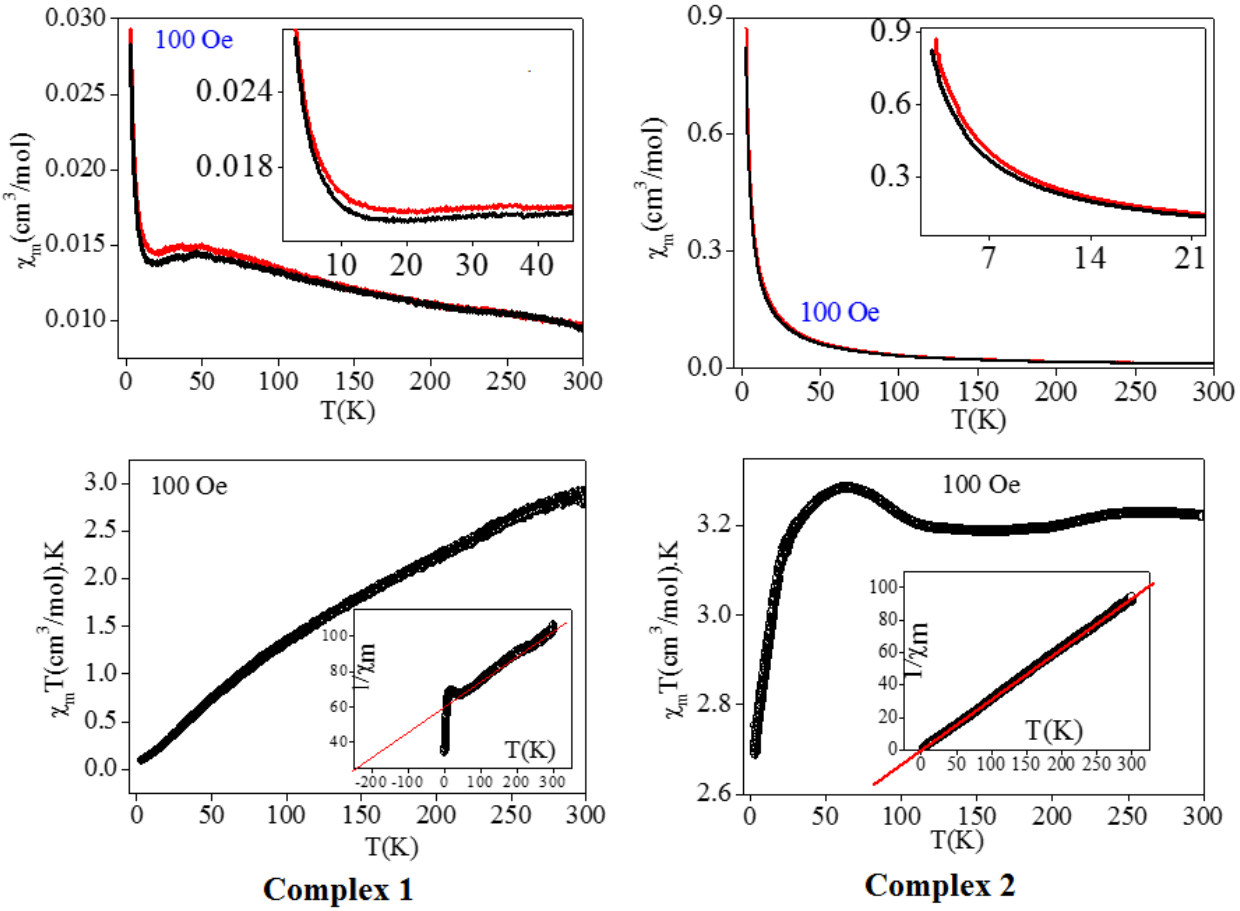

Fig. 2 The plot of molar susceptibility χ_m versus temperature from 3 to 300 K with 100 Oe applied external magnetic field for Cu_4O_4 clusters **1** and **2**. The inset shows the zoomed view at lower temperature showing very feeble bifurcation between ZFC-FC magnetization curves.

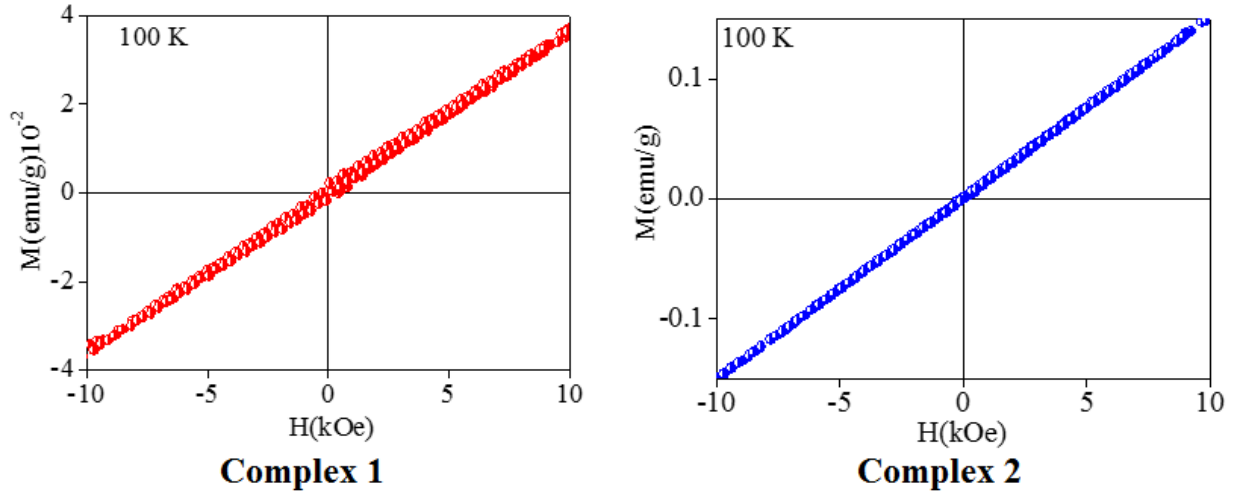

Fig. 3 M-H data at temperature 100 K for Cu_4O_4 clusters **1** and **2**. No coercivity was observed at 100 K and magnetization follows a linear relationship with the externally applied field.

3.6. Preliminary DNA binding studies

DNA is often a pharmacological target of most of the known anticancer drugs used for the treatment of solid cancers [27]. DNA-metal complex interactions play a significant role to dictate the possible mechanism of cell inhibition of drug entities and to evaluate the potential of chemical entities to act as drug candidates [28]. The binding of the complexes to CT-DNA/RNA and proteins is a pre-criteria for drug design and more insight into the cell death mechanism can be obtained by other enzymatic and cytotoxicity assays. We have studied copper cubane cluster **1** and **2** by many biophysical techniques *viz.* absorption, fluorescence, circular dichroism and thermal denaturation to validate their potential as drug entities. Briefly, we have summarized these preliminary studies in this section.

The binding propensity of **1** and **2** with CT-DNA was examined by employing absorption spectroscopy. After the successive addition of CT-DNA concentraions ($0.0 – 2.0 \times 10^{-4}$ M) to a Cu_4O_4 cubane clusters fixed concentrations (6.67×10^{-5} M), the π-π^* intraligand absorption band at 280 nm exhibited 'hyperchromism' along with a pertinent blue shift of 8-12 nm whereas LMCT band at 375 nm exhibited 'hypochromism' Fig. S12 and S13.

The strong hyperchromic effect (58 % and 62 % in **1** and **2**, respectively) whereas feeble % hypochromic effect of 24 % (**1**) and 30 % (**2**), revealed favorable electrostatic interaction of cationic polymetallic core to oxygen of sugar-phosphate (negatively charged) backbone of the DNA helix, as well as with the lively contribution of aromatic chromophores thorugh partial intercalation [29]. The cubane cluster topology gave a distinct isosbestic point at 299 nm in the presence of **1** and **2** indicative of equilibrium between the interacted Cu_4O_4 clusters and DNA double helix. Further, qualitative estimation of binding strengths of **1** and **2** with CT-DNA was established by the K_b values (intrinsic binding constant), obtained through Wolfe-Shimmer

equation [30]. The intrinsic binding constant K_b values for complex **1** and **2** were found to be $1.48 \pm 0.14 \times 10^4\ M^{-1}$ and $2.54 \pm 0.11 \times 10^4\ M^{-1}$, respectively, implicating strong binding affinity of Cu_4O_4 clusters with CT−DNA.

The fluorescence spectra of **1** and **2** exhibited a detectable fluorescence at *ca.* 350 nm when λ_{ex} = 280 nm. Further enhancement of the fluorescence was observed on substantial addition of CT-DNA ($0.0 - 1.8 \times 10^{-4}$ M) without any significant emission maxima shift (Fig. S14).

The binding strength of **1** and **2** with CT-DNA was determined by binding constant (*K*) values via Scatchard's equation [31] and were $4.41 \pm 0.17 \times 10^4\ M^{-1}$ and $8.78 \pm 0.12 \times 10^4\ M^{-1}$, respectively. The two-fold larger extent of binding propensity of **2** in comparison to **1** has been warranted by studying the frontier molecular orbital (HOMO and LUMO) analysis acquired through B3LYP/DFT calculations. Earlier literature accounts have established the evidence that the large HOMO energy of DNA and small LUMO energy of the molecules in contact directs quite higher binding affinity, since "electronic charge density" relocate with ease from DNA molecules (HOMO) to LUMO of molecule interacts and thus, a stronger interaction between DNA and the molecule happens [32]. Therefore, it was established that lower LUMO energy of the complex greater would be the binding affinity and here, complex **2** has lower LUMO energy (-1.60 eV) in comparison to complex **1** (-1.39 eV) as depicted in Fig. 4.

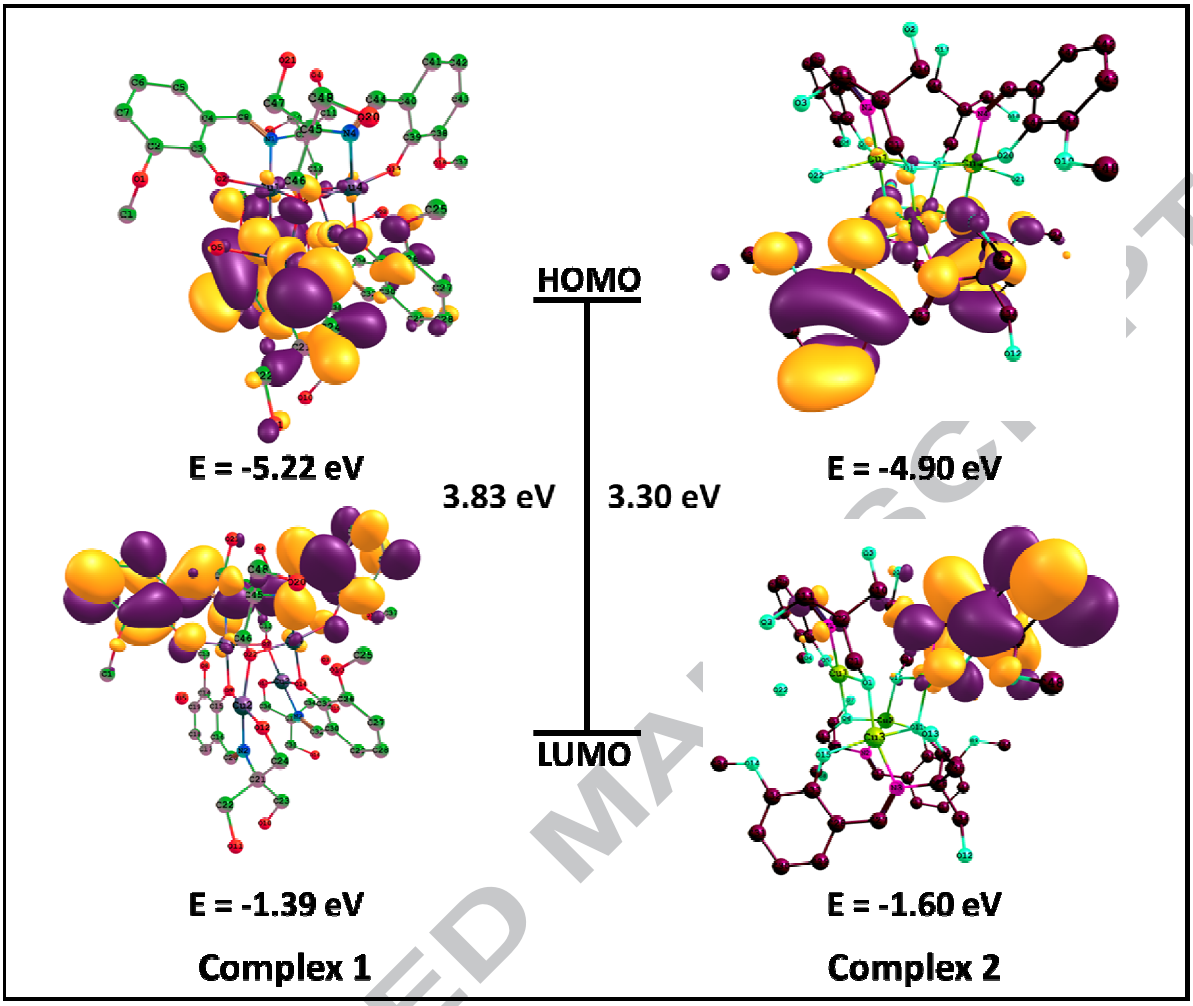

Fig. 4 Isodensity surfaces (isovalue 0.03) for the MOs of Cu_4O_4 clusters **1** and **2** were produced from the Kohn-Sham orbitals.

EB alone emits weak luminescence but in the presence of DNA, the EB-DNA complex emits strong luminescence that is because of intercalation of EB molecule planar phenenthridinium ring in between the adjacent base pairs of DNA. When **1** and **2** were added to DNA pretreated with EB, the induced emission intensity at 596 nm was quenched, Supporting Information, Fig. S15. The quenching of the fluorescence intensity upon the addition of the second molecule (complex **1** or **2**) was either due to the replacement of the bound EB or damage of the secondary structure of DNA. Since EB was not completely displaced, electrostatic interaction mode in

addition to the partial intercalation cannot be ruled out. Moreover, fluorescence quenching extent quantification was revealed by the Stern-Volmer equation [33]. The K_{sv} value for Cu_4O_4 clusters **1** and **2** was 2.42 ± 0.09 × 10^4 M^{-1} and 4.13 ± 0.06 × 10^4 M^{-1}, respectively following a similar trend as observed in K_b values.

The circular dichroic studies were employed to study the conformational changes observed due to Cu_4O_4 cubane clusters –DNA exchanges. The CD spectrum of CT-DNA exhibits characteristic B-type signature due to base stacking in the UV spectra at 276 nm (+ve band, UV: λ_{max}, 260 nm, CD [medg] 0.9602)) and 245 nm (-ve band, CD [medg] -0.8893) due to the B-DNA right-handed helicity (with a zero-crossover around 254 nm) which are quite sensitive to describe the mode of binding [34]. Upon successive addition of **1** and **2**, the +ve band intensity get reduced, (Fig. S16) which ascertain that **1** and **2** unwinds the DNA double helix and losses the helicity. The closed cubane cluster **2** showed more reduction in intensity of the CD band than **1** at the same concentration thus confirmed that topology of **2** (closed cubane clusters) is more efficient in disturbing the structure of DNA.

The amount of double-helical DNA strands transformed to single strands reduces to half at a particular temperature is known as the melting temperature "T_m". The unfolding of ds-DNA into ss-DNA determined by observed "hyperchromism" in the electronic absorption. At 260 nm, the molar extinction coefficient of ss-DNA is greater in comparison to ds-DNA [35]. The range of ΔT_m lies in between the value tempted for intercalative and electrostatic mode of binding. The intercalation stabilizes the DNA through π-π stacking that leads to substantial rise in the T_m of DNA, whereas the groove binding/electrostatic mode brings an slight deviation i.e. of 1-3 ˚C. [36].

For free CT-DNA, the T_m value was 80 ± 0.5 ˚C. The melting temperature (T_m) values in the presence of **1** and **2** were 84 ± 0.5 and 88 ± 0.5 ˚C. The observed ΔT_m value of 4-8 ˚C was similar to another groove binder along with the partial intercalators [37]. The melting profile of DNA in absence and presence of Cu_4O_4 cubane clusters **1** and **2** is depicted in Fig. S17.

3.7. DNA cleavage studies

To evaluate the DNA cleavage efficiency of Cu_4O_4 cubane clusters **1** and **2**, the plasmid DNA was treated with different concentrations of **1** and **2** in 5 mM Tris-HCl/NaCl buffer at pH 7.4 for 1 h without adding any reducing agents. With concomitant increase of **1** and **2**, Form I i.e., supercoiled form (SC) gets converted gradually into Form II i.e., nicked circular form (NC) (Lane 2-8 for **1** and 9-15 for **2**). At 35 μM concentration of **1** and **2** (Lane 6 for **1** and 11 for **2**), Form I was tranformed to Form II deprived of the formation of Form III i.e., linear circular form (LC) (Fig. 5). Thus, confirms the single-strand DNA cleavage by the complexes**1** and **2** [38].

The mechanistic pathway of cleavage of DNA by complexes **1** and **2** was studied being with the activators viz. hydrogen peroxide (H_2O_2), 3-mercaptopropionic acid (MPA), ascorbic acid (ASC), and glutathione (GSH). The DNA cleavage in presence of activators was significantly enhanced and follows order H_2O_2 > GSH > MPA > ASC (Fig. S18). Moreover, to enlighten the DNA cleavage mechanism, the interaction of **1** and **2** were studied in the company of ROS scavenger's viz. DMSO (dimethyl sulfoxide) and EtOH (ethanol) as hydroxyl radical scavengers, NaN_3 (sodium azide) as singlet oxygen quencher and SOD (superoxide dismutase) as superoxide scavengers (Fig. S19). From the electrophoretic pattern, it was perceived that DMSO and EtOH do not exhibits any deceptive inhibition of the DNA, thus rules out the prospect of diffusible hydroxyl radical's involvement in cleavage process. However, in addition of NaN_3 noteworthy

inhibition was noticed which confirms the presence of singlet oxygen, $^1O_2$. Thus, it confirms that DNA cleavages via oxidative path [39].

To further endorse binding of **1** and **2** with DNA, the cleavage reactions with, 4',6-diamidino-2-phenylindole (DAPI), a minor groove binder and methyl green (MG), a major groove binder, were studied (Fig. S19). No inhibition with DAPI was noticed while substantial inhibition of DNA cleavage with methyl green was observed point to the binding of Cu_4O_4 cubane clusters to the major groove of DNA. These results were further corroborated via molecular modelling studies.

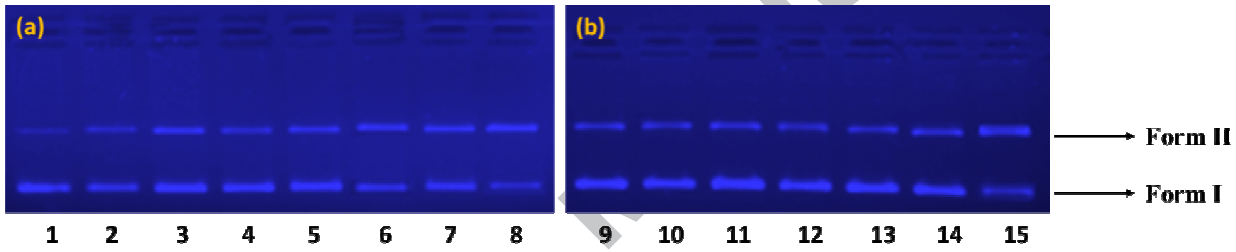

Fig. 5 Gel electrophoresis assay of Cu_4O_4 clusters **1** and **2** with pBR322 DNA in 5 mM Tris-HCl/NaCl buffer (pH, 7.4) after 1h incubation time. (a) Lane 1: DNA control; Lane 2: 5 μM 1 + DNA; Lane 3: 10 μM 1 + DNA; Lane 4: 15 μM 1 + DNA; Lane 5: 20 μM 1 + DNA; Lane 6: 25 μM 1 + DNA, Lane 7: 30 μM 1 + DNA, Lane 8: 35 μM 1 + DNA. (b) Lane 9: 5 μM 2 + DNA; Lane 10: 10 μM 2 + DNA; Lane 11: 15 μM 2 + DNA; Lane 12: 20 μM 2 + DNA; Lane 13: 25 μM 2+ DNA, Lane 14: 30 μM 2+ DNA, Lane 15: 35 μM 2+ DNA.

3.8. Molecular docking

To rationalize the topology of the specific binding interaction of Cu_4O_4 cubane clusters with DNA, the blind molecular docking was done, to simulate the interaction mode. In the present study, the structures of **1** and **2** were retained flexible to attain various conformations to predict best feasible minimum energy docked complex. The study revealed that major groove binding makes intimate contacts with the groove surface and as an outcome of this interaction numerous

electrostatic and van der Waals interactions occur between Cu_4O_4 cubane clusters and DNA bases and its sugar-phosphate backbone. By ensuing docked structures (Fig. 6-8), it is evident that both the cubane clusters **1** and **2**, slightly twists the interior hydrophobic surface of DNA in a way to make favorable contacts, the planar part of the aromatic rings stack between DNA base pairs and flexible alkyl alcohol arms lead to van der Waals and hydrophobic interactions with the outer surface of DNA, which are responsible for the stability of groove, detail are tabulated in Table S6. The relative binding propensity of docked structures was **1** (-4.8 kcal/mol) and **2** (-5.2 kcal/mol). Higher negative binding energy indicates a more stable association with DNA. Thus, it is concluded that the binding ability of **2** with the major groove of DNA is stronger than that of **1**.

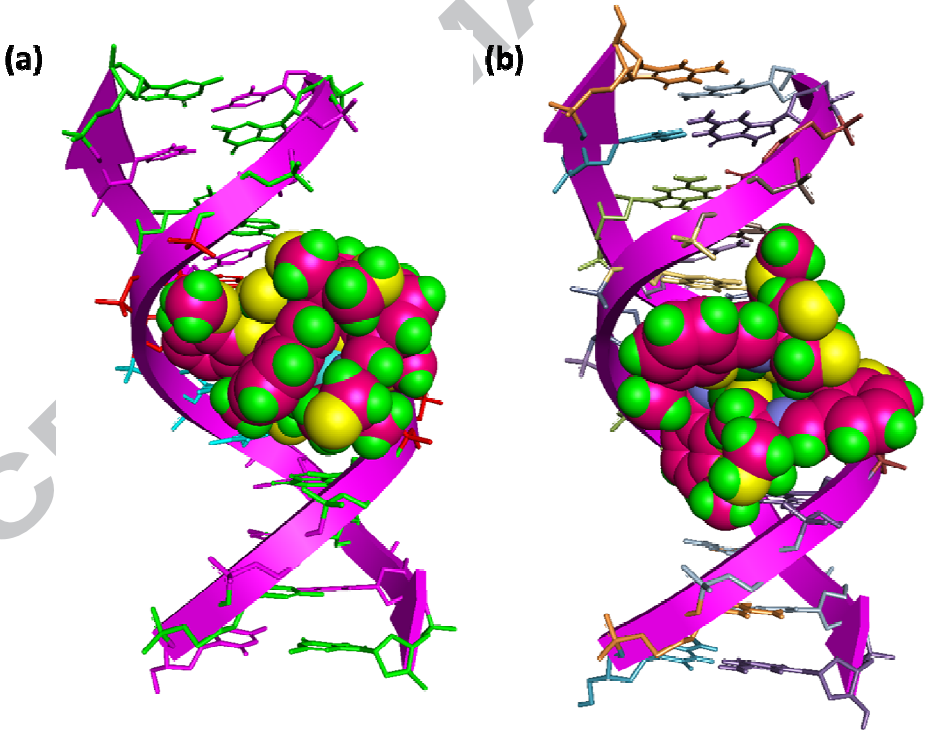

Fig. 6 Molecular docked structures of (a) Cu_4O_4 cluster **1**, and (b) Cu_4O_4 cluster **2** in the cavity of major groove of DNA.

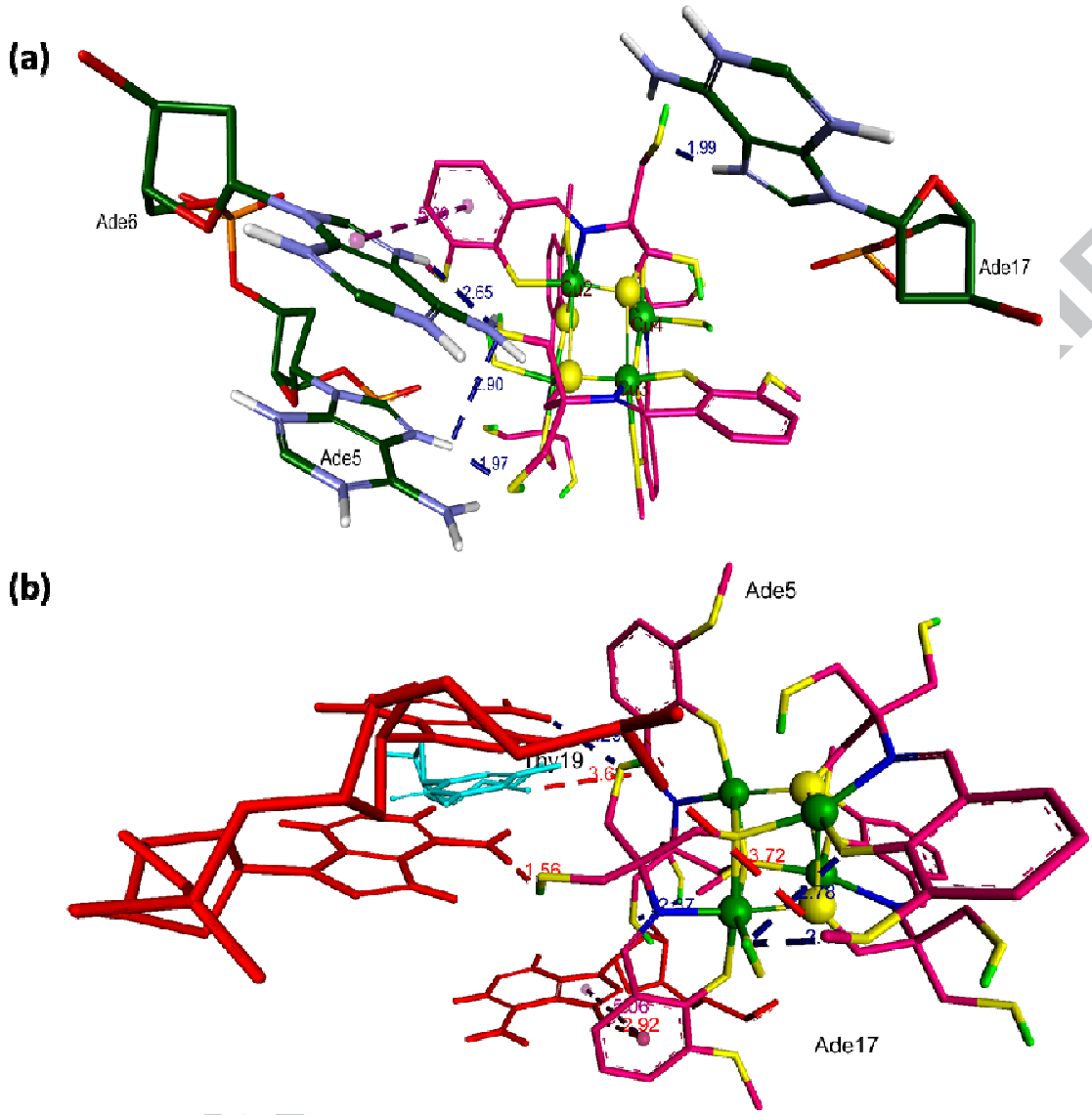

Fig. 7 Binding site non-covalent interactions minimum energy conformation of (a) Cu_4O_4 cluster **1** and (b) Cu_4O_4 cluster **2** with major groove residues.

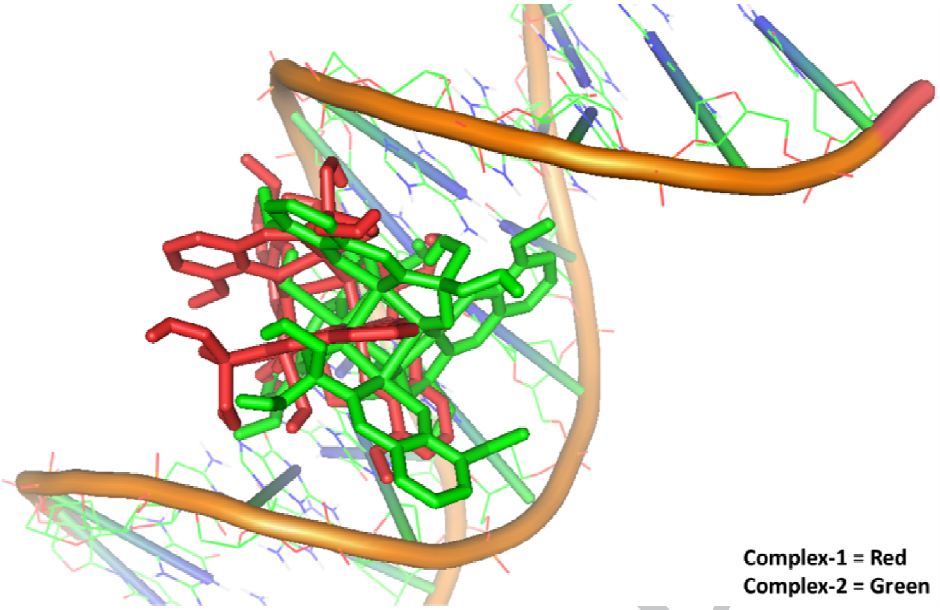

Fig. 8 Minimum energy docked pose of conformational binding site interaction differences between Cu_4O_4 clusters **1** and **2** in the major groove of the DNA.

3.9. Cytotoxicity activity

The cytotoxicity of copper cubane clusters **1** and **2** were tested on two human cancer cell lines, HepG2 and MCF-7 in concentration dependent fashion of cubane complexes (5–50 μM) by exposing cell for 24 h by MTT assay. Interestingly, our results demonstrate that **1** and **2** deliberated significant cytotoxic activity (IC_{50} value 20 and 17 μM, respectively) selectively towards MCF-7 breast cancer cell line. On the other hand, cytotoxicity activity of **1** and **2** on HepG2 cell line was moderate (IC_{50} value 35 and 30 μM, respectively). The changes observed in the morphology of the cell lines in MCF-7 and HepG2 cells on treatment with **1** and **2** after incubation 24 h are shown in Fig. 9.

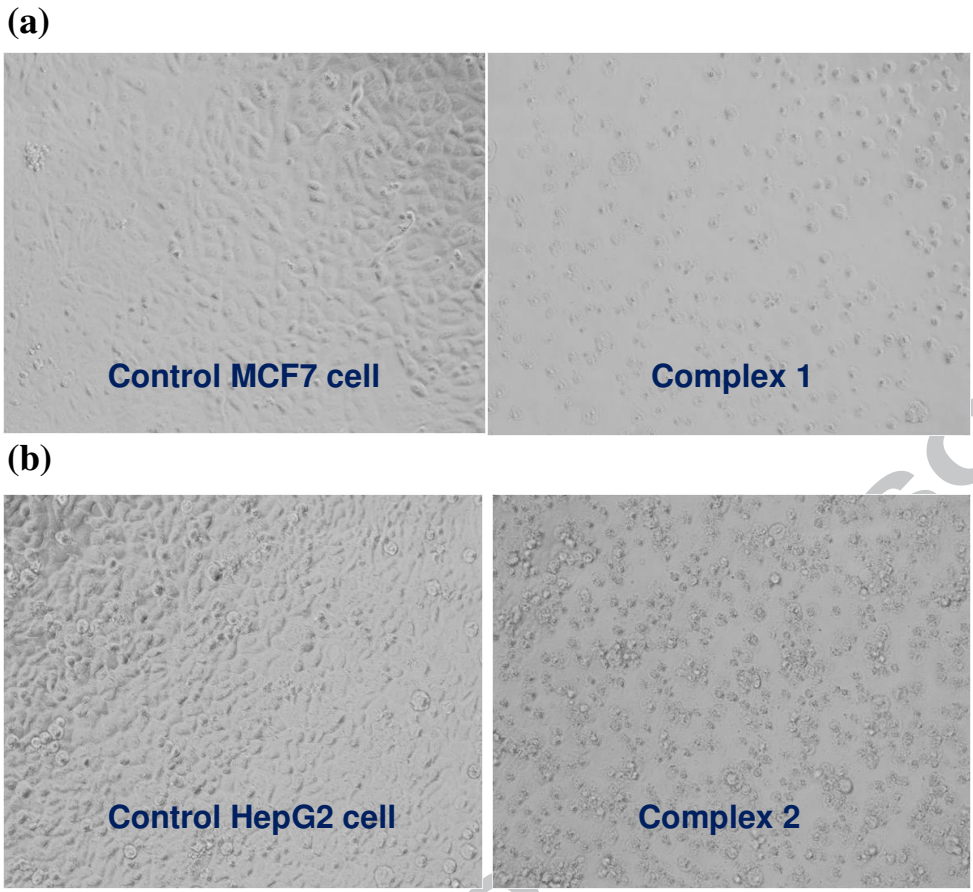

Fig. 9 (a) Morphological changes in MCF7 cells and **(b)** HepG2 cells, following the exposure of Cu_4O_4 clusters **1** and **2** for 24 h. Images were taken under the phase contrast inverted microscope at 20x magnification.

The morphology of MCF-7 and HepG2 cells on treatment with cubane clusters was found to be altered when observed in phase contrast inverted microscope. Upon exposure of compound to MCF-7 and HepG2 cells, there is a severe drop in the standard morphology and the cell adhesion capacity was noticed as compared with the control in concentration dependent pattern. However, the cytotoxicity of the compounds towards MCF-7 breast cancer cells is quite significant attributable to the particular target-oriented selectivity that can be ascribed to the ligand and the

Cu_4O_4 metallic core high electron density, by which the DNA-binding propensity also gets facilitated [40].

3.10. ROS generation in cell apoptosis

It is well known that metallo-anticancer drugs, mainly copper complexes, exhibit their anticancer prpoperty because of reactive oxygen species (ROS) generation, viz. superoxide anion radical ($O_2^{\bullet-}$), and hydroxyl radical ($OH^{\bullet}$) [41]. Generally, Cu(I) ions reduces hydrogen peroxide to form hydroxyl radical ($OH^{\bullet}$) whereas Cu(II) ions get reduced to Cu(I) by the superoxide anion ($O_2^{\bullet-}$) or glutathione (GSH). The formation of ROS viz. $OH^{\bullet}$ is copper compelled, irrespective of the oxidation state of copper hosted inside the body. The existence of additional intracellular ROS could lead to severe DNA damage in cells. The intracellular ROS generation extent in MCF-7 cells was observed upon treatment of **1** and **2** and by monitoring fluorescence intensity of DCFH-DA. The results showed triggered ROS generation and the pattern exhibited was also dose-dependent (Fig. 10), which confirmed that ROS generation and their role in the cell apoptosis.

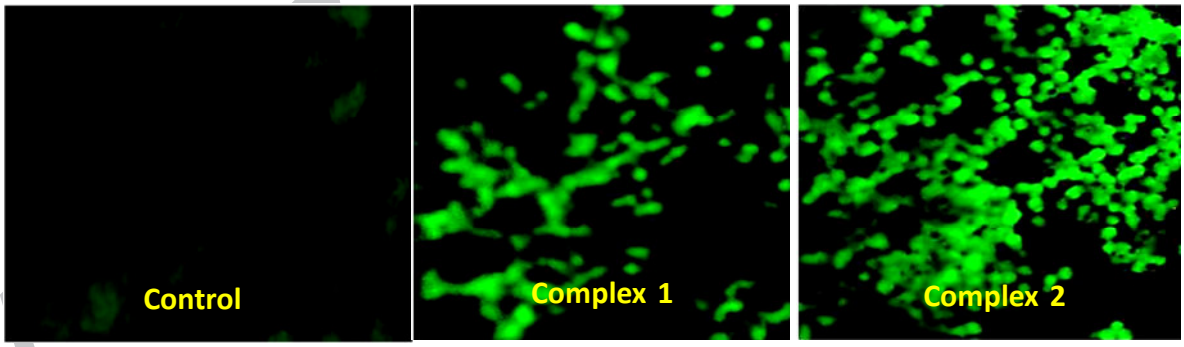

Fig. 10 ROS generation in MCF-7 (breast cancer cell lines) after the treatment of 20 μM of the complexes **1** and **2** for 24 h.

3.11. Intracellular glutathione depletion

For the oxidative stress inside the cells, an intracellular antioxidant glutathione (GSH) is present for protection. In vivo, Cu(II) ions get reduced to Cu(I) by GSH / superoxide anion ($O2^{\bullet-}$). A specific copper transporter (hCtr) is known to take Cu(I) inside the cell. This enables the independent penetration of copper complexes, without the need of any binding to any other agent. To find out the role of oxidative stress in the cytotoxicity, the impact on intracellular GSH level is an important parameter. It is well known that the effect of Cu(II) complex produces a noteworthy drop in GSH level. The GSH/GSSG ratio affects the regulation of cell cycle, DNA synthesis, and mutagenic processes in cancer cells. The GSH level is found to be in the higher range in cancer cells in comparison to normal cells. The GSH level of **1** and **2** at concentrations of 15 and 20 μM was quantified in MCF-7 cell lines after exposure for 24 h. The results are depicted in the histogram (Fig. 11). The depletion in the level of GSH was found upon treatment of **1** and **2** which was attributed to the presence of four Cu(II) ions in Cu_4O_4 cubane core clusters. Interestingly, **2** which is a closed cubane cluster and possess relatively less energy separation in HOMO and LUMO (as evidenced by DFT) exhibited more significant results and showed the reduced intracellular GSH level to 45% at a concentration of 20 μM, thus endorsing the important role of oxidative stress by cubane clusters.

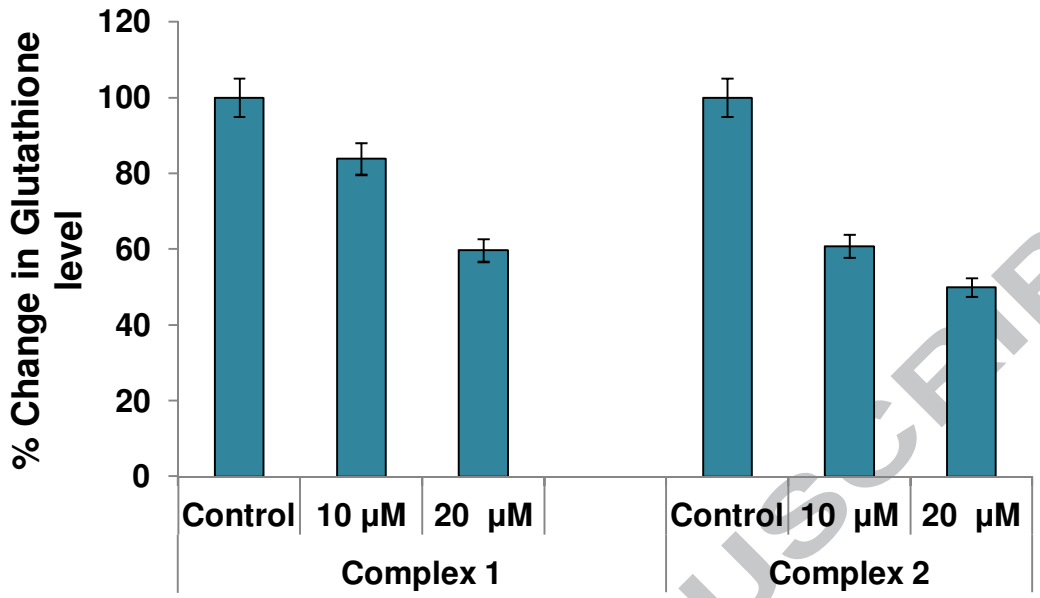

Fig. 11 Glutathione depletion in MCF-7 cells exposed to Cu_4O_4 clusters **1** and **2** for 24 h.

3.12. Lipid peroxidation

Another essential parameter to ascertain the role of oxidative damage is the level of lipid peroxidation inside the cell. The oxidative stress is known to damage the cell membrane as well as the cell organelles viz. mitochondria via lipid peroxidation. The amount of malondialdehyde (MDA, a lipid peroxidation end product) determines the degradation of lipids, by adopting TBARS (Thiobarbituric Acid Reactive Substance) assay [42]. A substantial increase is depicted in lipid peroxidation (Fig. 12) in the presence of **1** and **2** in MCF-7 breast cancer cells treated for 24 h in a concentration-dependent pattern.

There was an exponential rise in lipid peroxidation 60% and 40%, respectively on treating **1** and **2** (20 µM) in MCF-7 cells while **2** registered a more prominent rise in lipid peroxidation as compared to **1** well corroborated with GSH assay pattern. All these biological assays which include cleavage activity mediated by an oxidative pathway involving ROS species, intracellular

GSH depletion, and lipid peroxidation up-regulation intensely implicate cellular damage induced by **1** and **2** in MCF-7 cancer cell lines. This is the first demonstration of antitumor-active Cu_4O_4 cubane clusters **1** and **2** against MCF-7 to best of our knowledge which bears novelty to act as target-oriented specific chemotherapeutics for the treatment of breast cancers and warrant further investigations for phase I clinical trials.

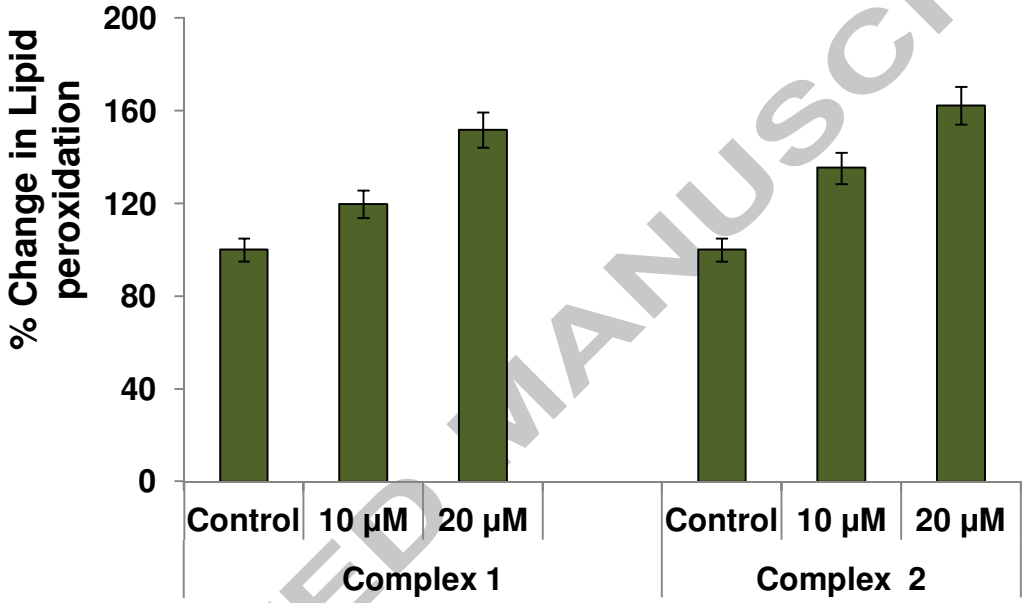

Fig. 12 Lipid peroxidation level in MCF-7 cells exposed to Cu_4O_4 clusters **1** and **2** for 24 h.

4. Conclusions

Two new tetranuclear Cubane Cu_4O_4 cluster complexes $[Cu_4(H_2L)_4{\cdot}2H_2O]{\cdot}5H_2O$ (**1**) and $[Cu_4(H_2L)_4{\cdot}(H_2O)_4]$ (**2**) were synthesized as potential antitumor chemotherapeutic agents. Both the compounds **1** and **2** were thoroughly characterized by single X-ray crystallography and various other spectroscopic practices. The Cu_4O_4 cluster, **1** possesses open cubane-like core in which the four copper atoms are bridged by two phenolate oxygen and two alkoxo oxygen atoms from $\mathbf{H_2L^{2-}}$ ligands while in **2**, four copper centers are mutually interconnected via four oxygen

atoms of alkoxo of four H_2L^{2-} ligand moieties to produce a distorted single-closed cubane core with S4-symmetry. The temperature dependent magnetic susceptibility measurements showed antiferromagnetic and ferromagnetic nature for **1** and **2**, respectively. The i*n vitro* DNA interation profile of Cu_4O_4 clusters demonstrated typical hyperchromic shift in UV-vis absorptions stuides with CT-DNA, symptomatic of the cationic polymetallic core to the oxygen atoms of sugar-phosphate (anionic part) electrostatic binding, additionally to energetically contributing aromatic chromophores via partial intercalation between adjacent base pairs of DNA double helix. The perceived two-fold larger degree of binding of **2**, in comparison with **1** can be warranted by the possessions of lower LUMO energy of **2**. The mechanistic track of cell death was examined via DNA cleavage, intracellular GSH depletion and LPO assays. The complexes **1** and **2** demonstrate DNA cleavage via an oxidative mechanism influenced by ROS viz. $O_2^{\cdot-}$, $^1O_2$. *In vitro* cytotoxic activity confirmed that both complexes **1** and **2** exhibited significantly noteworthy activity against MCF-7 (breast cancer) cell lines and displayed moderate results on HepG2 (liver cancer) cell lines. Moreover, on exposure of **1** to MCF-7 and HepG2 cell lines, ROS and TBARS levels were significantly amplified which was interconnected to the reduction of GSH levels. Thus, these studies validate the potential of **1** and **2** for specific targeted chemotherapeutic intervention, particularly in the case of MCF-7 breast carcinomas and warrants further *in vivo* investigations.

Acknowledgements

The authors are grateful to SAIF Punjab University, Chandigarh, for providing ESI–MS and elemental analysis facility. We are also thankful to Department of Chemistry and USIF, Aligarh Muslim University for providing the FT-IR, UV-vis, and EPR facility. Authors thankful the staff of IIT-Roorkee for the assistance in Single Crystal X-ray studies. The authors extend their

appreciation to the Deanship of Scientific Research at King Saud University for funding this work through research group No. RG-1438-006. Mohammad Usman sincerely acknowledges financial support from University Grants Commission (UGC), New Delhi, for providing the fellowship and the Department of Chemistry, AMU through UGC assisted DRS–SAP, DST-FIST, and DST PURSE Programme.

References

(1) (a) R. H.Holm, P. Kennepohl and E. I. Solomon, Chem. Rev. 96 (1996) 2239–2314. (b) E. I. Solomon, U. M. Sundaram and T. E. Machonkin, Chem. Rev. 96 (1996) 2563–2606. (c) R. G. Hadt, D. Hayes, C. N. Brodsky, A. M. Ullman, D. M. Casa, M. H. Upton, D. G. Nocera and L. X. J. Chen, Am. Chem. Soc. 138 (2016) 11017–11030. (d) R. Papadakis, E. Riviere, M. Giorgi, H. Jamet,` P. Rousselot-Pailley, M. Reglier, A. J. Simaan and T. Tron, Inorg. Chem. 52 (2013) 5824–5830.

(2) (a) E. Ruiz, P. Alemany, S. Alvarez and J. Cano, J. Am. Chem. Soc. 119 (1997) 1297–1303. (b) R. E. P. Winpenny, Dalton Trans. 2002, 1-10. (c) S. S. P. Dias, V. Andre, J. Kłak, M. T. Duarte and A. M. Kirillov, Cryst. Growth Des. 14 (2014) 3398–3407. (d) A. M. Kirillov, M. V. Kirillova and A. J. L. Pombeiro, Coord. Chem. Rev. 256 (2012) 2741-2759. (e) D. A. Whittington and S. J. Lippard, J. Am. Chem. Soc. 123 (2001) 827-838.

(3) (a) K. Isele, P. Franz, C. Ambrus, G. Bernardinelli, S. Decurtins and A. F. Williams, Inorg. Chem. 44 (2005) 3896–3906. (b) K. Tercero, E. Ruiz, S. Alvarez, A. Rodriguez Fortea and P. Alemany, J. Mater. Chem. 2006, 2729–2735. (c) A. Mukherjee, R. Raghunathan, M. K. Saha, M. Nethaji, S. Ramasesha and A. R. Chakravarty, Chem. Eur. J. 11 (2005) 3087–3096. (d) A. Burkhardt, E. T. Spielberg, H. Görls and W. Plass, Inorg. Chem. 47 (2008) 2485–2493.

(4) (a) S. Thakurta, P. Roy, R. J. Butcher, M. S. E. Fallah, J. Tercero, E. Garribba and S. Mitra, Eur. J. Inorg. Chem. (2009) 4385–4395. (b) E. Gungor, H. Kara, E. Colacio and A. J. Mota, Eur. J. Inorg. Chem. 2014, 1552–1560.

(5) (a) Y. Song, C. Massera, O. Roubeau, P. Gamez, A. M. M. Lanfredi and J. Reedijk, Inorg. Chem. 43 (2004) 6842-6842. (b) Q. Benito, X. F. Le Goff, S. B. Maron, A. Fargues, A. Garcia,

C. Martineau, F. Taulelle, S. Kahlal, T. Gacoin, J. P. Boilot and S. Perruchas, J. Am. Chem. Soc. 136 (2014) 11311−11320. (c) G. A. Ardizzoia and S. Brenna, Coord. Chem. Rev. 311 (2016) 53–74.

(6) R. Mergehenn and W. Haase, Acta Cryst., Sect. B 33 (1977) 1877-1882.

(7) (a) H. Pagonda, P.P. Yogesh, H.R. Katreddi, N. Munirathinam. Inorg. Chim. Acta, 392, (2012) 478-484. (b) J. Sun, C. Tessier, R.H. Holm. Inorg. Chem., 46 (2007) 2691–2699. (c) Y. Zhao, J. Zhu, W. He, Z. Yang, Y. Zhu, Y. Li, J. Zhang, Z. Guo Chem. Eur. J., 12 (2006) 6621-6629.

(8) (a) C. Liu, M. Wang, T. Zhang and H. Sun, Coord. Chem. Rev. 248 (2004) 147-168. (b) A. Patra, T. K. Sen, A. Ghorai, G. T. Musie, S. K. Mandal, U. Ghosh and M. Bera, Inorg. Chem. 52 (2013) 2880−2890. (c) K. J. Humphreys, K. D. Karlin and S. E. Rokita, J. Am. Chem. Soc. 124 (2002) 8055. (d) J. Hernandez-Gil, S. Ferrer, A. Castineiras and F. Lloret, Inorg. Chem. 51 (2012) , 9809−9819.

(9) (a) M. Niu, Z. Li, H. Li, X. Li, J. Dou and S. Wang, RSC Adv. 5 (2015) 37085–37095. (b) M. Niu, D.W. J. Sun, H. H. Li, Z.Q. Cao, S. N. Wang and J. M. Dou, J. Coord. Chem. 67 (2014) 81–95.

(10) (a) G.C. Giri, S. Haldar, L. Carrella, A.B. Panda, G.T. Musie and M. Bera, Polyhedron, 99 (2015), 7–16. (b) S. Tabassum, M. Afzal, H. Al–Lohedan, M. Zaki, R. A. Khan, and M. Ahmad, *Inorganica Chimica Acta*, 463 (2017) 142-155. (c) R. Vafazadeh, A.C. Willis. J. Coord. Chem., 68 (2015) 2240-2252. (d) R. Vafazadeh, F. Jafari, M.M. Heidari, A.C. Willis. J. Coord. Chem., 69 (2016) 1313-1325.

(11) (a) F. Neese, The ORCA program system. WIREs Comput. Mol. Sci. 2 (2012) 73−78.

(12) (a) C. Lee, W. Yang and R. G. Parr, Phys. Rev. B. 37 (1988) 785–789. (b) F. Weigend and R. Ahlrichs, Phys. Chem. Chem. Phys. 7 (2005) 3297–3305. (c) A. Schaefer, C. Huber and R. Ahlrichs, J. Chem. Phys. 100 (1994) 5829-5835. (d) A. Schaefer, H. Horn and R. Ahlrichs, J. Chem. Phys. 97 (1992) 2571-2577.

(13) (a) S. Grimme, J. Antony, S. Ehrlich and H. Krieg, J. Chem. Phys. 2010, 132. (b) C. Steffen, K. Thomas, U. Huniar, A. Hellweg, O. Rubner and A. Schroer, J. Comput. Chem. 31 (2010) 2967–2970.

(14) (a) O. Trott and A. J. Olson, J. Comput., Chem., 31 (2010) 455-461. (b) M. F. Sanner, J. Mol. Graphics Mod., 17 (1999) 57-61.

(15) (a) Accelrys Software Inc., Discovery Studio Modeling Environment, Release 4.0, San Diego: Accelrys Software Inc., 2013. (b) The PyMOL Molecular Graphics System, Version 1.5.0.4 Schrödinger, LLC.

(16) International Tables for X-Ray Crystallography; Kynoch Press: Birmingham, England, 1952; Vol. III.

(17) SAINT, version 6.02; Bruker AXS: Madison, WI, 1999. (c) Sheldrick, G. M. SADABS: Empirical Absorption Correction Program; University of Göttingen: Göttingen, Germany, 1997.

(18) XPREP, version 5.1; Siemens Industrial Automation Inc.; Madison, WI, 1995.

(19) G. M. Sheldrick, SHELXTL Reference Manual, version 5.1; Bruker AXS: Madison, WI, 1997.

(20) (a) G. M. Sheldrick, SHELXL-97: Program for Crystal Structure Refinement; University of Göttingen: Göttingen, Germany, 1997. (b) G.M. Sheldrick, *Acta Cryst.*, **C27** (2015) 3-8.

(21) (a) M. Usman, F. Arjmand, M. Ahmad, M. S. Khan, I. Ahmad and S. Tabassum, Inorg. Chim. Acta, 453 (2016) 193–201. (b) W. M. A. Asbahy, M. Usman, F. Arjmand, M. Shamsi and S. Tabassum, Inorg. Chim. Acta, 445 (2016) 167-178. (c) M. Usman, M. Zaki, R. A. Khan, A. Alsalme, M. Ahmad and S. Tabassum, RSC Adv., 7 (2017) 36056-36071.

(22) I. Yousuf, F. Arjmand, S. Tabassum, L. Toupet, R. A. Khan, and M. A. Siddiqui, Dalton Trans., 44 (2015) 10330-10342 and reference therein.

(23) (a) R. A. Khan, S. Yadav, Z. Hussain, F. Arjmand, S. Tabassum, Dalton Trans., 43 (2014) 2534–2548. (b) R. A. Khan, A.de Almeida, K. Al-Farhan, A. Alsalme, A. Casini, M.Ghazzali, J. Reedijk, J. Inorg. Biochem. 165 (2016) 128–135. R. A. Khan, K. Al-Farhan, A.de Almeida, A. Alsalme, A. Casini, M.Ghazzali, J. Reedijk, J. Inorg. Biochem. 140 (2014) 1–5

(24) (a) R. A. Khan, M. Usman, D. Rajakumar, P. Balaji, A. Alsalme, F.Arjmand, K. Al Farhan, M. A. Akbarsha, F.Marchetti, C. Pettinari, and S. Tabassum. Scientific Rep. 7 (2017) 45229. (b) S. Tabassum A. Asim, R. A. Khan, F. Arjmand, D. Rajakumar, P. Balaji, M. A. Akbarsha, RSC Adv., 5 (2015) 47439-47450.

(25) D. Chandra, K. V. Ramana, L. Wang, B. N. Christensen, A. Bhatnagar and S. K. Srivastava, Invest. Ophthalmol. Visual Sci. 43

(26) J. A. Buege and S. D. Aust, Methods Enzymol. 52 (1978) 302–310.

(27) (a) A. M. Pyle and J. K. Barton, Prog. Inorg. Chem. 38 (1990) 413–475. (b)) T. D. Tullius, American Chemical Society: Washington, DC, 1989. (c) C. X. Zhang and S. Lippard, J. Curr. Opin. Chem. Biol. 7 (2003) 481-489.

(28) (a) A. C. Komor and J. K. Barton, Chem. Commun. 49 (2013) 3617–3630. (b) C. Santini, M. Pellei, V. Gandin, M. Porchia, F. Tisato and C. Marzano, Chem. Rev. 114 (2014) 815–862. (c) A. N. Kate, A. A. Kumbhar, A. A. Khan, P. V. Joshi and V. G. Puranik, Bioconjugate Chem. 25 (2014) 102–114.

(29) (a) M. Ganeshpandian, R. Loganathan, E. Suresh, A. Riyasdeen, M.A. Akbarshad and M. Palaniandavar, Dalton Trans. 43 (2014) 1203-1219. (b) R. Manikandan, Y. J. Chitrapriya, N. Jang and P. Viswanathamurthi, RSC Adv., 3 (2013) 11647-11657.

(30) A. Wolfe, G. H. Shimer and T. Meehan, Biochemistry. 26 (1987) 6392-6396.

(31) E. F. Healy, J. Chem. Educ. 84 (2007) 1304–1307.

(32) (a) H. Sugiyama and I. Saito, J. Am. Chem. Soc. 118 (1996) 7063-7068. (b) N. Kurita and K. Kobayashi, Comput. Chem. 24 (2000) 351-357.

(33) J. R. Lakowicz, and G. Weber, Biochemistry. 24 (1973) 4171- 4179.

(34) R. Loganathan, S. Ramakrishnan, E. Suresh, M. Palaniandavar, A. Riyasdeen and M. A. Akbarsha, Dalton Trans. 43 (2014) 6177–6194.

(35) O. Novakova, H. Chen, O. Vrana, A. Rodger, P.J. Sadler and V. Bravec, Biochemistry. 42 (2003) 11544–11554.

(36) V. A. Kawade, A. A. Kumbhar, A. S. Kumbhar, C. Nather, A. Erxleben, U. B. Sonawane and R. R. Joshi, Dalton Trans. 40 (2011) 639–650.

(37) K. J. Akerman, A. M. Fagenson, V. Cyril, M. Taylor, M. T. Muller, M. P. Akerman and O. Q. Munro, J. Am. Chem. Soc. 136 (2014) 5670–5682.

(38) X. Qiao, Z. Y. Ma, C. Z. Xie, F. Xue, Y. W. Zhang, J. Y. Xu, Z. Y. Qiang, J.S. Lou, G.J. Chen and S.P. Yan, J. Inorg. Biochem. 105 (2011) 728–737.

(39) (a) M. S. Melvin, M. W. Calcutt, R. E. Noftle and R. A. Manderville, Chem. Res. Toxicol. 15 (2002) 742-748. (b) Q. Jiang, N. Xiao, P. Shi, Y. Zhu and Z. Guo, Coord. Chem. Rev. 251 (2007) 1951–1972.

(40) (a) K. J. Humphreys, K. K. Karlin and S. E. Rokita, J. Am. Chem. Soc. 123 (2001) 5588-5589; (b) K. J. Humphreys, K. K. Karlin and S. E. Rokita, J. Am. Chem. Soc. 124 (2002) 6009-

6019; (c) M. P. Suh, M. Y. Han, J. H. Lee, K. S. Min and C. Hyeon, J. Am. Chem. Soc. 120 (1998) 3819-3820.

(41) (a) C. Marzano, M. Pellei, F. Tisato and C. Santini, Med. Chem. 9 (2009) 185–211. (b) F. Tisato, C. Marzano, M. Porchia, M. Pellei and C. Santini, Med. Res. Rev. 30 (2010) 708–749.

(42) (a) A. Linden, M. Gülden, H. J. Martin, E. Maser and H. Seibert, Toxicol. in Vitro. 22 (2008) 1371–1376. (b) H. H. Draper and M. Hadley, Methods Enzymol. 186 (1990) 421–431.

TOC:

Two new tetranuclear cubane (open and closed) with Cu_4O_4 core complexes were synthesized and fully characterized. The in-vitro cytotoxicity assays of the complexes against MCF7 and HepG2 human cancer cell lines.

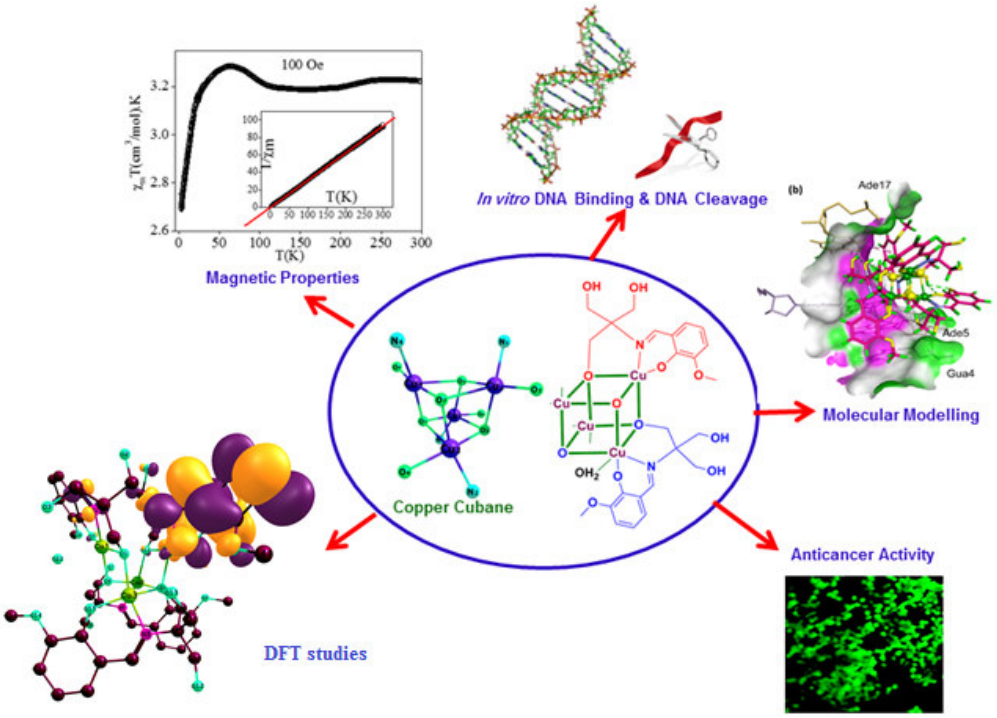

Highlights

- Two new tetranuclear cubane (open and closed) with Cu_4O_4 core complexes.
- X-ray diffraction, Magnetism, Computational Chemistry
- *In vitro* DNA binding studies, cleavage, Molecular docking
- *In-vitro* cytotoxicity against MCF7 human cancer cell lines.